J. Fluid Mech. (2009), *vol.* 635, *pp.* 439–454.
doi:10.1017/S0022112009007770

The forced motion of a flag

A. MANELA[1]† AND M. S. HOWE[2]

[1]Department of Mathematics, Massachusetts Institute of Technology, Cambridge, MA 02139, USA

[2]Boston University, College of Engineering, 110 Cummington Street, Boston, MA 02215, USA

(Received 2 December 2008; revised 21 April 2009; accepted 22 April 2009)

The prevailing view of the dynamics of flapping flags is that the onset of motion is caused by temporal instability of the initial planar state. This view is re-examined by considering the linearized two-dimensional motion of a flag immersed in a high-Reynolds-number flow and taking account of forcing by a 'street' of vortices shed periodically from its cylindrical pole. The zone of nominal instability is determined by analysis of the self-induced motion in the absence of shed vorticity, including the balance between flag inertia, bending rigidity, varying tension and fluid loading. Forced motion is then investigated by separating the flag deflection into 'vortex-induced' and 'self' components. The former is related directly to the motion that would be generated by the shed vortices if the flag were absent. This component serves as an inhomogeneous forcing term in the equation satisfied by the 'self' motion. It is found that forced flapping is possible whenever the Reynolds number based on the pole diameter $Re_D \gtrsim 100$, such that a wake of distinct vortex structures is established behind the pole. Such conditions typically prevail at mean flow velocities significantly lower than the critical threshold values predicted by the linear theory. It is therefore argued that analyses of the onset of flag motion that are based on ideal, homogeneous flag theory are incomplete and that consideration of the pole-induced fluid flow is essential at all relevant wind speeds.

1. Introduction

The mechanics of a flag in a uniform stream constitutes a fundamental fluid-structure interaction that has been studied extensively (Païdoussis 1998). Its relative simplicity and richness of behaviour make it relevant to a wide range of natural phenomena and problems of engineering importance. For example, Huang (1995) has applied the flag equation to study the flutter mechanism governing snoring. Watanabe *et al.* (2002*a*, *b*) have investigated the dynamics of paper flutter and demonstrated its importance in amending production processes in commercial printing. Similarly, Liao *et al.* (2003) have demonstrated how the flapping mechanism improves propulsive efficiency of swimming, and Shen *et al.* (2003) have shown that wavy body motions may help in reducing turbulent drag during locomotion.

These and other studies have motivated both experimental and theoretical investigations. Taneda (1968) examined the waving motions of flags in a wind tunnel. Zhang *et al.* (2000) and Zhu & Peskin (2002) studied the problem using an analogous system of flexible filaments in flowing soap films. Fitt & Pope (2001) have studied the case of a 'stiff' flag in air incident at a finite angle of attack. Shelley, Vandenberghe &

† Email address for correspondence: avshalom@math.mit.edu

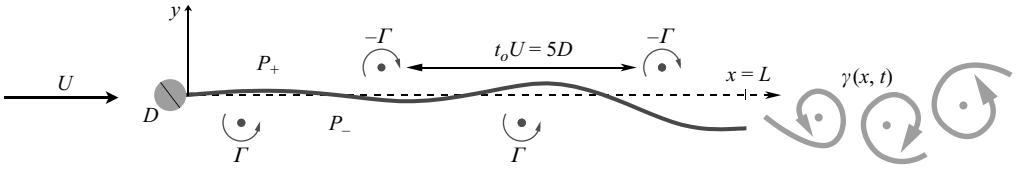

FIGURE 1. Schematic set-up of the problem. The flag is pinned at $x = 0$ to a stationary cylindrical pole of diameter D and its free end is at $x = L$. The inertial fluid loading is $\Delta P = P_- - P_+$ and the trailing-edge vorticity is $\gamma(x, t)$. The vortices shed from the flag pole are each of strength $\Gamma \approx 2.5UD$ and convect along $y = \pm h \approx \pm 0.45D$ at speed U.

Zhang (2005) performed flag experiments in a water tunnel and compared their results to 'heavy-flag' analysis. Argentina & Mahadevan (2005) proposed a linearized flag theory involving a simplified model of the pressure loading based on thin airfoil theory (Milne-Thomson 1968). Tang & Païdoussis (2007) studied, in addition to the onset of instability, the post-critical behaviour of the system and compared it with existing experimental data. Connell & Yue (2007) addressed the full nonlinear problem and solved it numerically in conjunction with the incompressible viscous Navier–Stokes equations. Alben & Shelley (2008) solved the inviscid nonlinear problem coupled with the dynamics of the trailing edge vortex sheet wake. Eloy *et al.* (2008) considered the three-dimensional problem and found it in better agreement with experiments. Manela & Howe (2009) applied the approximate Argentina–Mahadevan model to study the effect of varying the boundary conditions and calculated the sound generated by the motion.

The common view in all of these studies is that flapping results from temporal instability of an initial planar state. The threshold of instability is marked by a critical value of the wind speed and determined from the solution of a homogeneous eigenvalue problem. The equation of motion consists of a balance between flag inertia, bending rigidity, tension force and fluid loading. External forcing is disregarded; in particular, forcing by disturbances in the viscous wake of the flag pole are ignored.

Several works have studied the motion of a flexible filament placed in the wake of a bluff body. Among the first to observe the usefulness of such motions were Taylor *et al.* (2001), who suggested to convert the kinetic energy of these motions into electric power by using a piezoelectric 'eel' as the flapping filament. Allen & Smith (2001) examined experimentally the feasibility of this idea and found conditions for optimal coupling between the wake and filament characteristics. Unlike in the flag problem set-up (see figure 1), the flexible structure in this study is located at some distance downstream from the bluff body. Other investigators, including Beal *et al.* (2006) and Eldredge & Pisani (2008), studied the effectiveness of the wake-induced motions in enabling passive locomotion.

Following this group of studies, the objective of the present work is to investigate the effect of the flag pole wake on the flag motion. We argue that a proper theory of flapping should incorporate the influence of the flag pole wake. The characteristics of the wake depend on Reynolds number based on the effective diameter of the pole. For a smooth, circular cylindrical pole of diameter D in a steady stream of speed U the Reynolds number

$$Re_D = UD/\nu,$$

where ν is the kinematic viscosity (Blevins 1990). At moderate flow speeds, the wake consists of a succession of distinct vortex structures (roughly aligned with

the flag pole) typically when $Re_D \gtrsim 100$. For a pole of diameter $D = 0.05\,\mathrm{m}$ in air, $\nu \approx 15 \times 10^{-6}\,\mathrm{m^2\,s^{-1}}$ and therefore $Re_D \approx 3.3 \times 10^3 U$ (U in $\mathrm{m\,s^{-1}}$). Consequently, discrete vortices would be expected downstream of the flag pole when U exceeds $\sim 0.03\,\mathrm{m\,s^{-1}}$. At higher mean wind speeds, common in both outdoor and laboratory experiments, the vortex wake is sufficiently established to be modelled in a first approximation by two parallel quasi-periodic vortex 'streets' over the opposite faces of the flag. The vortex circulation $\Gamma \approx 2.5UD$ and the characteristic frequency f_0 of the shedding satisfies $f_0 D/U \approx 0.2$ (Griffin & Ramberg 1975, Blevins 1990). The corresponding period $t_0 = 1/f_0$ during which two vortices of opposite sign are released is $t_0 \approx 5D/U$.

In this paper a simple double vortex sheet model of this kind is used to approximate the resulting linearized motion of the flapping flag. This model neglects any 'back-reaction' of the flag motion on the motion of the vortices (see § 5). By consideration of the homogeneous (or unforced) problem, it is shown that flapping induced by the flag pole wake is always significant at subcritical wind speeds (given that the pole diameter is finite), at which the unforced flag would be nominally stable. In other words, the effect of forcing by wake vorticity is important at all relevant wind speeds, and stability criteria that fail to take account of the vortex shedding are probably of little practical significance. A linearized representation of the flag equation of motion is formulated in § 2, and solutions are sought in § 3 with and without account taken of the vortex wake. Numerical results are presented in § 4, where the relative contributions of flag inertia, tension and bending stiffness are discussed.

2. The governing equations

Consider a uniform incompressible flow at velocity $\mathbf{U} = \hat{\mathbf{i}}U$ parallel to an inextensible flag of length L and mass per unit area ρ_s (figure 1). The flag is pinned to a flag pole of diameter D whose axis coincides with the z-axis of the rectangular coordinates (x, y, z). The flag has thickness λ and span l, with $\lambda \ll L \ll l$, such that the motion may be regarded as two-dimensional in planes of constant z. Attention is confined to the high-Reynolds-number regime ($Re_L = UL/\nu \gg 1$) where the boundary layers on the flag may be regarded as fully developed turbulent, inducing a mean flag tension

$$T = 2\rho_0 u_*^2 (L - x), \tag{2.1}$$

where ρ_0 is the fluid density, x is measured along the flag from the pole in the direction of the mean stream and $u_* \sim 0.037U$ is the friction velocity (Hinze 1975). In practice, the turbulent nature of the flow over the surfaces arises because the flag pole 'trips' the boundary layer, so that a dynamically steady mean turbulence state is established over a short distance downstream of the pole. In addition, a real flag is rough enough to promote further turbulence production at the surface. Once the steady state is established the friction velocity becomes approximately constant and the tension will vary linearly with distance. Small-amplitude unsteady deflections of the flag (in the y direction) of amplitude $\xi(t, x) \ll L$ are taken to satisfy the linearized equation

$$\rho_s \frac{\partial^2 \xi}{\partial t^2} + EI \frac{\partial^4 \xi}{\partial x^4} - \frac{\partial}{\partial x}\left(T \frac{\partial \xi}{\partial x}\right) - \Delta P = 0, \tag{2.2}$$

where EI is the flag bending rigidity (E being the Young's modulus and $I = \lambda^3/12(1-\sigma^2)$ the moment of inertia per unit span, σ is the Poisson ratio of the material) and ΔP denotes the pressure force across the flag in the direction of increasing ξ.

2.1. *The fluid loading* ΔP

The pressure jump ΔP is attributable to an irrotational part ΔP_I associated with the potential flow induced by the motion of the flag together with a wake-induced component ΔP_γ arising from vortices released from the trailing edge of the flag. Following Argentina & Mahadevan (2005) we adopt the following approximation for the potential ϕ_I on the surface of the flag produced by the motion of the flag

$$\phi_I \approx \pm\sqrt{x(L-x)}\left(\frac{\partial \xi}{\partial t} + U\frac{\partial \xi}{\partial x}\right), \quad y = \pm 0. \tag{2.3}$$

This is precisely the result obtained from classical airfoil theory (Bisplinghoff, Ashley & Halfman 1955) applied to a rigid airfoil, for which the normal velocity $v_n = \partial\xi/\partial t + U\partial\xi/\partial x$ is constant along the airfoil surface. Argentina & Mahadevan (2005) argue that (2.3) provides a good first approximation to the exact potential provided the deflections of the flag are small and v_n varies slowly along the flag, corresponding to the systematic neglect of terms $\sim O(\partial^2\xi/\partial x\partial t)$ and higher. The approximation neglects the influence on ϕ_I of 'non-local' flag motions whose effects are controlled by these higher order derivatives. A more careful treatment would take account of interactions at a distance by replacing the flag by a distribution of sources, as described, for example, by Bisplinghoff *et al.* (1955), and involves integration of v_n along the flag.

Argentina & Mahadevan (2005) used the above approximation to predict the minimum mean flow velocity at which a flag becomes unstable in cases where vortex shedding from the flag pole does not occur. These predictions were systematically about 50 %–70 % of the critical velocities measured by Watanabe *et al.* (2002) for a flag attached to a thin wire of negligible radius. In what follows (§ 4) it will be shown that the effect of vortex shedding from the flag pole is to practically reduce the critical velocity to a very small value at which shedding from the pole becomes established ($Re_D \sim 100$). Thus, for our purposes, the use of the Argentina–Mahadevan model (defined in (2.3)), although involving errors of detail, will not affect in any essential way the qualitative conclusions of the analysis.

The application of Bernoulli's equation to (2.3) and the neglect of terms $O(\partial^2\xi/\partial x^2, \partial^2\xi/\partial x\partial t)$ in accord with the above approximation yield the non-circulatory pressure jump in the form

$$\Delta P_I = \frac{\rho_0 U(2x-L)}{\sqrt{x(L-x)}}\left(\frac{\partial \xi}{\partial t} + U\frac{\partial \xi}{\partial x}\right) - 2\rho_0\sqrt{x(L-x)}\frac{\partial^2 \xi}{\partial t^2}, \tag{2.4}$$

which contains the typical inverse square-root leading- and trailing-edge singularities together with the conventional added-mass term, represented by the last term in (2.4). The velocity will remain finite at the trailing edge of the flag provided an appropriate amount of vorticity is released continuously within a downstream wake. This wake is modelled by a vortex sheet of circulation $\gamma = \gamma(x,t)$ per unit length (where $L < x < \infty$, see figure 1). The corresponding circulatory pressure jump ΔP_γ produced by this wake (Argentina & Mahadevan 2005) is

$$\Delta P_\gamma = -\frac{L(2C(\gamma)-1) + 2x(1-C(\gamma))}{\sqrt{x(L-x)}}\left(\frac{\partial \xi}{\partial t} + U\frac{\partial \xi}{\partial x}\right), \tag{2.5}$$

where $C(\gamma)$ is the Theodorsen function (Theodorsen 1935),

$$C(\gamma) = \frac{\displaystyle\int_L^\infty \frac{x}{\sqrt{x^2 - L^2}}\gamma(x,t)\,\mathrm{d}x}{\displaystyle\int_L^\infty \sqrt{\frac{x+L}{x-L}}\gamma(x,t)\,\mathrm{d}x}. \tag{2.6}$$

The total pressure jump is therefore

$$\Delta P = \Delta P_I + \Delta P_\gamma = -2\rho_0 U C(\gamma)\sqrt{\frac{L-x}{x}}\left(\frac{\partial \xi}{\partial t} + U\frac{\partial \xi}{\partial x}\right) - 2\rho_0\sqrt{x(L-x)}\frac{\partial^2 \xi}{\partial t^2}. \tag{2.7}$$

2.2. *Equation of motion forced by flag pole vortices*

Vortex shedding from the flag pole will be represented by two 'streets' of discrete line vortices assumed to be released periodically from the flag pole and to be convected in the mean wind over the surfaces of the flag (figure 1). The vortices have circulation $\mp\Gamma$ ($\Gamma > 0$) and respectively assumed to convect along $y = \pm h$. A vortex released at time $t = 0$ is represented formally by

$$\boldsymbol{\omega} = \mp \boldsymbol{k}\,\Gamma\delta(y \mp h)\delta(x - Ut), \tag{2.8}$$

where $\boldsymbol{k}$ is a unit vector in the positive z direction (out of the plane of figure 1) and δ denotes the Dirac delta function. The vortex (2.8) is decomposed into frequency components by writing

$$\boldsymbol{\omega} = \int_{-\infty}^{\infty} \boldsymbol{\omega_p} \exp\left[-\mathrm{i}\omega t\right] \mathrm{d}\omega, \tag{2.9}$$

where

$$\boldsymbol{\omega_p} = \mp\frac{\boldsymbol{k}\Gamma}{2\pi U}\,\delta(y \mp h)\exp[\mathrm{i}\omega x/U],\ x > 0. \tag{2.10}$$

The vorticity distribution (2.10) represents a vortex sheet extending over the semi-infinite region $0 < x < \infty$. It produces irrotational motion at points not on the sheet described by a potential ϕ_ω, say. If we approximate ϕ_ω by the corresponding potential that occurs when the sheet extends over $-\infty < x < \infty$, then the appropriate solution of Laplace's equation supplies

$$\phi_\omega = \frac{\Gamma}{4\pi\mathrm{i}\omega}\exp[-\mathrm{i}\omega(t - x/U) \pm |\omega|(y \mp h)/U],\ |y| < h. \tag{2.11}$$

This formula can be used to calculate the corresponding fluid displacement ξ_p induced at the mean position of the flag by means of the relation

$$\frac{\mathrm{D}\xi_\omega}{\mathrm{D}t} \equiv \frac{\partial \xi_\omega}{\partial t} + U\frac{\partial \xi_\omega}{\partial x} = \frac{\partial \phi_\omega}{\partial y}|_{y=0}, \tag{2.12}$$

i.e.

$$\frac{\partial \xi_\omega}{\partial t} + U\frac{\partial \xi_\omega}{\partial x} = \pm\frac{\Gamma\,\mathrm{sign}(\omega)}{4\pi\mathrm{i}U}\exp[-\mathrm{i}\omega(t - x/U) - |\omega|h/U]. \tag{2.13}$$

The resulting solution for ξ_ω is not valid close to the flag pole, where the contributions from vorticity in $x < 0$ would be significant. However, the following particular integral of (2.13)

$$\xi_{\omega_\pm}(x, t - x/U, \omega) = \pm\frac{\Gamma\,\mathrm{sign}(\omega)}{4\pi\mathrm{i}U^2}x\exp[-\mathrm{i}\omega(t - x/U) - |\omega|h/U], \tag{2.14}$$

in which the ξ_{ω_+} and ξ_{ω_-} respectively correspond to vortices below and above the flag, vanishes at the pole ($x \to +0$), so that the error near the pole cannot be very large. Indeed, an approximation of the kind (2.14) is probably the best and most convenient possible on linear theory, because the actual behaviour of $\xi_{\omega_\pm}$ near the pole involves a complex interaction between partially shed vorticity and the rigid surface of the pole and would not be properly represented even by the semi-infinite vortex sheet (2.10).

The overall 'vortex-induced' deflection $\xi_p(x, t-x/U)$ is given by integration of (2.14) over all frequencies $(-\infty, \infty)$ and by summing the contributions from all vortices

$$\xi_p(x, t-x/U) = \sum_{n=-\infty}^{\infty} \int_{-\infty}^{\infty} \xi_{\omega_+}(x, t-nt_0, \omega)\,\mathrm{d}\omega + \sum_{n=-\infty}^{\infty} \int_{-\infty}^{\infty} \xi_{\omega_-}(x, t-(2n+1)t_0/2, \omega)\,\mathrm{d}\omega, \quad (2.15)$$

where t_0 is the period during which two vortices of opposite sign are released. An explicit expression for ξ_p is calculated in (3.17).

We may now use these results to formulate a 'forced' equation of motion of the flag in the presence of the flag pole vortices. Let the overall flag deflection ξ be partitioned into its 'self' and 'vortex-induced' parts:

$$\xi(x, t-x/U) = \xi_o(x, t-x/U) + \xi_p(x, t-x/U), \quad (2.16)$$

and substitute this into (2.2), in which T is given by (2.1). In the linearized approximation vortices convecting in the mean flow do not produce a pressure load on the flag. The equation for ξ_o therefore assumes the inhomogeneous form

$$\rho_s \frac{\partial^2 \xi_o}{\partial t^2} + EI \frac{\partial^4 \xi_o}{\partial x^4} - 2\rho_0 u_*^2 \frac{\partial}{\partial x}\left((L-x)\frac{\partial \xi_o}{\partial x}\right) - \Delta P(\xi_o) = F_e(\xi_p), \quad (2.17)$$

where

$$F_e(\xi_p) = -\rho_s \frac{\partial^2 \xi_p}{\partial t^2} - EI \frac{\partial^4 \xi_p}{\partial x^4} + 2\rho_0 u_*^2 \frac{\partial}{\partial x}\left((L-x)\frac{\partial \xi_p}{\partial x}\right). \quad (2.18)$$

2.3. *End conditions*

Four boundary conditions are required to complete the formulation of the problem. We consider here a 'supported-free' flag, which satisfies

$$(\xi)_{x=0} = \left(\frac{\partial^2 \xi}{\partial x^2}\right)_{x=0} = \left(\frac{\partial^2 \xi}{\partial x^2}\right)_{x=L} = \left(\frac{\partial^3 \xi}{\partial x^3}\right)_{x=L} = 0\,; \quad (2.19)$$

the displacement and bending moment vanish at the pole, and the free end is moment- and force-free. These conditions differ from the commonly used 'clamped-free' conditions, where the condition of zero moment at the pole is replaced by the requirement that the angle of deflection should vanish (Huang 1995; Zhang *et al.* 2000; Watanabe *et al.* 2002*a*, *b*; Zhu & Peskin 2002; Argentina & Mahadevan 2005; Shelley *et al.* 2005). In general, the nature of the end conditions has a strong influence on the profile of the resulting flag motion in the absence of flag pole vortices (Manela & Howe 2009). It is our contention that a constraint on the bending moment at the pole (which in practice may be non-zero but small) better reflects conditions in practice than a requirement on the angle of deflection, and will therefore adopt this type of condition here.

3. Analysis

3.1. *The homogeneous response:* $F_e = 0$

A non-dimensional representation of the problem is obtained by normalizing distances with respect to the flag length L and by adopting the non-dimensional time $\bar{t} = Ut/L$. The resulting equation is

$$\frac{\partial^2 \bar{\xi}_h}{\partial \bar{t}^2} + \frac{1}{\alpha^2}\frac{\partial^4 \bar{\xi}_h}{\partial \bar{x}^4} - \frac{c_*}{\mu}\frac{\partial}{\partial \bar{x}}\left((1-\bar{x})\frac{\partial \bar{\xi}_h}{\partial \bar{x}}\right) - \frac{1}{\mu}\Delta \bar{P} = 0, \tag{3.1}$$

where the bars denote non-dimensional quantities, and where

$$\mu = \rho_s/\rho_0 L \quad \text{and} \quad \alpha = U/U_b, \tag{3.2}$$

are respectively the non-dimensional flag mass density and the normalized wind speed ($U_b = \sqrt{EI/\rho_s L^2}$ being a characteristic bending wave velocity), and $c_* = 2u_*^2/U^2 \approx 2.74 \times 10^{-3}$ which may be regarded as a fixed 'friction factor' (see (2.1) *et seq.*). Typical values of μ and α for a polyester flag ($E \approx 3$ Gpa, $\sigma \approx 0.3$) of thickness $\lambda \approx 10^{-4}$ m and mass density $\rho_s \approx 0.4$ kg m^{-2} in air ($\rho_0 \approx 1.3$ kg m^{-3}) are $\mu \approx 0.3/L$ and $\alpha \approx 40LU$ (numerical values measured in SI units). Thus $\mu \approx 0.3$ and $\alpha \approx 40U$ for a flag of length $L = 1$ m. In a typical experimental set-up one is usually interested in determining the critical, or minimum, velocity (corresponding to the critical value of α) at which flapping first occurs.

The time-harmonic solution,

$$\bar{\xi}_h(\bar{x}, \bar{t}) = \bar{\zeta}_h(\bar{x}) \exp[-\mathrm{i}\bar{\omega}_h \bar{t}], \tag{3.3}$$

of (3.1) has been examined by Manela & Howe (2009) for $c_* = 0$ (no tension). Substitution of (3.3) into (3.1) results in an eigenvalue problem which is solved by expanding the solution in a series of orthonormal functions (obtained from the balance of inertia and elasticity terms in (3.1)) that satisfy the boundary conditions (2.19). The solution yields an expression for the neutral surface

$$\mathrm{Im}\{\bar{\omega}_h(\mu, \alpha, \mathrm{Re}\{\bar{\omega}_h\})\} = 0, \tag{3.4}$$

determining the instability boundary in the (μ, α) plane.

When $c_* \neq 0$ in (3.1) the calculation is slightly modified, but the basic steps in the numerical evaluation of (3.4) are identical to those described by Manela & Howe (2009). The details of calculation are not reproduced here because our focus is on the motion forced by the vortex wake of the flag pole and, in addition, subsequent results indicate that flag tension hardly affects the stability of the unforced flag (see § 4.1 and figure 2).

3.2. *Motion forced by flag pole vortices*

The inhomogeneous equation (2.17) is solved by introducing the Fourier time transform $\hat{g}(\bar{x}, \bar{\omega})$ of a function $\bar{g}(\bar{x}, \bar{t})$ according to the definition

$$\hat{g}(\bar{x}, \bar{\omega}) = \frac{1}{2\pi}\int_{-\infty}^{\infty} \bar{g}(\bar{x}, \bar{t}) \exp[\mathrm{i}\bar{\omega}\bar{t}]\, \mathrm{d}\bar{t}. \tag{3.5}$$

The transformed non-dimensional equation is

$$-\bar{\omega}^2 \hat{\xi}_o + \frac{1}{\alpha^2}\hat{\xi}_o'''' - \frac{c_*}{\mu}((1-\bar{x})\hat{\xi}_o')' - \frac{1}{\mu}\Delta \hat{P}(\hat{\xi}_o) = \hat{F}_e(\hat{\xi}_p), \tag{3.6}$$

where

$$\Delta\hat{P}(\hat{\xi}_o) = -2C(\gamma)\sqrt{\frac{1-\bar{x}}{\bar{x}}}(-\mathrm{i}\bar{\omega}\hat{\xi}_o + \hat{\xi}_o') + 2\bar{\omega}^2\sqrt{\bar{x}(1-\bar{x})}\hat{\xi}_o, \tag{3.7}$$

and primes denote differentiation with x. In (2.6) we put

$$\bar{\gamma}(\bar{x},\bar{t}) = \bar{\gamma}_0(\bar{\omega})\exp\left[\mathrm{i}\bar{\omega}(\bar{t}-\bar{x}/2)\right] \tag{3.8}$$

to obtain

$$C(\bar{\omega}) = \frac{\displaystyle\int_1^\infty \frac{\bar{x}}{\sqrt{\bar{x}^2-1}}\exp\left[-\mathrm{i}\bar{\omega}\bar{x}/2\right]\mathrm{d}\bar{x}}{\displaystyle\int_1^\infty \sqrt{\frac{\bar{x}+1}{\bar{x}-1}}\exp\left[-\mathrm{i}\bar{\omega}\bar{x}/2\right]\mathrm{d}\bar{x}}. \tag{3.9}$$

When $\bar{\omega}$ is real we find (Theodorsen 1935)

$$C\,(\bar{\omega}) = \frac{H_1^{(2)}\,(\bar{\omega}/2)}{H_1^{(2)}\,(\bar{\omega}/2) + \mathrm{i}H_0^{(2)}\,(\bar{\omega}/2)} \tag{3.10}$$

where $H_i^{(2)}$ are Hankel functions of the second kind and ith order.

The forcing term in (3.6) is

$$\hat{F}_e(\hat{\xi}_p) = \bar{\omega}^2\hat{\xi}_p - \frac{1}{\alpha^2}\hat{\xi}_p'''' + \frac{c_*}{\mu}((1-\bar{x})\hat{\xi}_p')', \tag{3.11}$$

where $\hat{\xi}_p$ is given from (2.14) and (2.15) by (see, e.g. Lighthill 1958)

$$\hat{\xi}_p(\bar{x},\bar{\omega}) = \frac{\Gamma\bar{x}}{\mathrm{i}UL}\exp[\mathrm{i}\bar{\omega}\bar{x} - |\bar{\omega}|h/L]\sum_{n=0}^{\infty}[\delta(\bar{\omega}-(2n+1)\bar{\omega}_0) - \delta(\bar{\omega}+(2n+1)\bar{\omega}_0)], \tag{3.12}$$

and $\bar{\omega}_0 = 2\pi/\bar{t}_0 = 2\pi L/5D$ is the non-dimensional angular frequency of the release of each pair of vortices of opposite sign. In accordance with (3.12), assume

$$\hat{\xi}_o(\bar{x},\bar{\omega}) = \frac{\Gamma\bar{\zeta}(\bar{x},\bar{\omega})}{\mathrm{i}UL}\exp[\mathrm{i}\bar{\omega}\bar{x} - |\bar{\omega}|h/L]\sum_{n=0}^{\infty}[\delta(\bar{\omega}-(2n+1)\bar{\omega}_0) - \delta(\bar{\omega}+(2n+1)\bar{\omega}_0)], \tag{3.13}$$

and substitute into (3.6) together with (3.11) and (3.12) to yield an equation for $\bar{\zeta}(\bar{x},\bar{\omega})$. The end conditions (2.19) are to be satisfied by the *sum* of $\hat{\xi} = \hat{\xi}_o + \hat{\xi}_p$. Taking Fourier transforms these become

$$\hat{\xi}_o(0) = -\hat{\xi}_p(0),\ \hat{\xi}_o''(0) = -\hat{\xi}_p''(0),\ \hat{\xi}_o''(1) = -\hat{\xi}_p''(1),\ \hat{\xi}_o'''(1) = -\hat{\xi}_p'''(1). \tag{3.14}$$

The substitution of (3.13) and (3.12) into (3.14) supplies the required end conditions for $\bar{\zeta}(\bar{x},\bar{\omega})$. The problem obtained for $\bar{\zeta}(\bar{x},\bar{\omega})$ is outlined in the Appendix. Note that when the influence of the pressure loading term is relatively small (i.e. when bending rigidity is large or when the flag is heavy) the solution reduces to $\hat{\xi}_o \approx -\hat{\xi}_p$, and the total deflection $\hat{\xi} = \hat{\xi}_o + \hat{\xi}_p$ vanishes. This observation will be used later to rationalize the motion of 'stiff' and 'heavy' flags (see figure 6).

The solution $\bar{\zeta}(\bar{x},\bar{\omega})$ is obtained numerically by Chebyshev collocation (Peyret 2002). This method transforms (A 1) of the Appendix and the boundary conditions (A 3) into a system of N linear algebraic equations of the form

$$\boldsymbol{A}\bar{\boldsymbol{\zeta}} = \boldsymbol{B}, \tag{3.15}$$

satisfied respectively at N collocation points along the flag. Here $\boldsymbol{A}(\bar{\omega})$ is a matrix representing the differential operator acting on $\bar{\zeta}$, $\boldsymbol{B}(\bar{\omega})$ is the forcing vector and $\boldsymbol{\zeta}$ is

the vector of unknown values of $\bar{\zeta}$ at the discrete collocation points. Our calculations indicate that excellent convergence of the numerical scheme is achieved throughout the parameter domain for $N \lesssim 60$.

The solution $\bar{\zeta}(\bar{x}, \bar{\omega})$ is used in (3.13) to determine $\hat{\bar{\xi}}_o(\bar{x}, \bar{\omega})$. Because $\bar{\zeta}(\bar{x}, \bar{\omega}) = \text{c.c.}\{\bar{\zeta}(\bar{x}, -\bar{\omega})\}$ (see (A 1)–(A 3)), the 'self' deflection of the flag is given by the inverse Fourier transform

$$\bar{\bar{\xi}}_o(\bar{x}, \bar{t} - \bar{x}) = \int_{-\infty}^{\infty} \hat{\bar{\xi}}_o(\bar{x}, \bar{\omega}) \exp[-\mathrm{i}\bar{\omega}\bar{t}]\mathrm{d}\bar{\omega} = \frac{2\Gamma}{UL} \sum_{n=0}^{\infty} (\mathrm{Re}\{\bar{\zeta}(\bar{x}, \bar{\omega}_n)\} \times \sin[\bar{\omega}_n(\bar{t} - \bar{x})] + \mathrm{Im}\{\bar{\zeta}(\bar{x}, \bar{\omega}_n)\} \cos[\bar{\omega}_n(\bar{t} - \bar{x})]) \times \exp[-\bar{\omega}_n h/L], \quad (3.16)$$

where $\bar{\omega}_n = (2n + 1)\bar{\omega}_0$. A similar calculation using (3.12) yields

$$\bar{\bar{\xi}}_p(\bar{x}, \bar{t} - \bar{x}) = \int_{-\infty}^{\infty} \hat{\bar{\xi}}_p(\bar{x}, \bar{\omega}) \exp[-\mathrm{i}\bar{\omega}\bar{t}]\, \mathrm{d}\bar{\omega} = \frac{2\Gamma\bar{x}}{UL} \sum_{n=0}^{\infty} \sin[\bar{\omega}_n(\bar{t} - \bar{x})] \exp[-\bar{\omega}_n h/L]. \quad (3.17)$$

This completes the formal calculation of the overall forced response $\bar{\bar{\xi}} = \bar{\bar{\xi}}_o + \bar{\bar{\xi}}_p$.

4. Numerical results

4.1. *The homogeneous response*

Our primary objective is to study the forced motion of the flag. However, it is important to delineate the zone of instability in the absence of shedding from the flag pole, because it is our contention that forcing at subcritical conditions puts in question the relevance of the homogeneous temporal stability problem.

Figure 2 illustrates the neutral surface (3.4) in (a) the (μ, α) plane and (b) the $(\mu, \mathrm{Re}\{\bar{\omega}_h\})$ plane. The solid lines correspond to the full solution and the dashed curves mark the neutral surface in the absence of drag-induced tension obtained by Manela & Howe (2009). The shaded zone in figure 2(*a*) marks the domain of stability. For each value of $\mu = \rho_s/\rho_0 L$ there exists a critical normalized wind speed $\alpha = U/U_b = \alpha_c$ above which instability sets in. The value of α_c increases monotonically with μ, confirming the intuitive result that heavier flags require stronger wind to flap. The critical frequency $\mathrm{Re}\{\bar{\omega}_h\}$ at which instability is excited can be found from the corresponding point in figure 2(*b*). This frequency decreases when μ increases, showing that heavier flags start flapping at lower frequencies. At subcritical conditions ($\alpha < \alpha_c$ for fixed μ) the flag is stable and all eigenvalues lie in the lower half of the complex $\bar{\omega}_h$ plane. At $\alpha = \alpha_c$, the lowest eigenmode becomes neutrally stable (with $\mathrm{Im}\{\bar{\omega}_h\} = 0$) and for $\alpha > \alpha_c$ instability sets in as a propagating wave with time-increasing amplitude.

Both parts of figure 2 show that the shape of the neutral surface is only marginally dependent on flag tension. The introduction of the drag-tension force increases the value of α_c by less than 1 %, presumably because of the small value of the friction coefficient $c_* \approx 2.74 \times 10^{-3}$ in (3.1). This may be contrasted with results of Argentina & Mahadevan (2005), who predicted that α_c increases by about 20 % when tension is included for a 'clamped-free' flag. Apart from the different end conditions, this difference may be a consequence of the laminar boundary layer used by these authors (as opposed to the present turbulence induced drag (2.1)) and the apparently incorrect form of their tension term (assumed to be a constant) in (1) of Argentina & Mahadevan (2005).

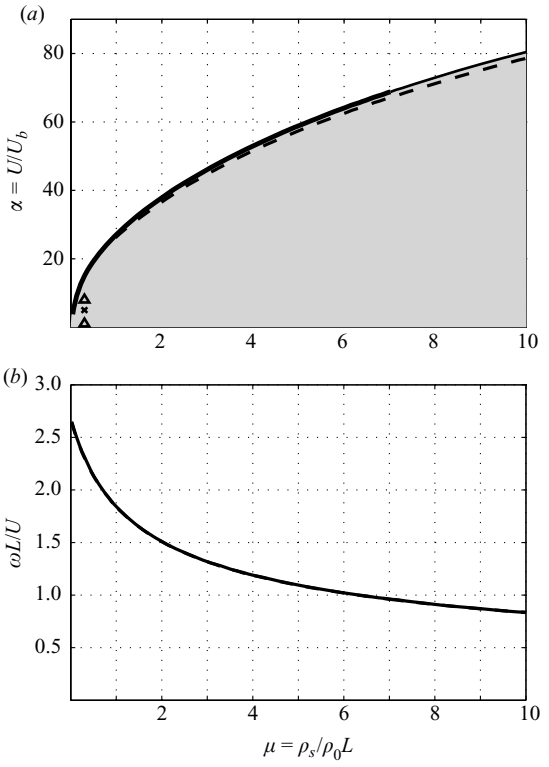

FIGURE 2. The projections of the neutral surface on the (a) (μ, α) and (b) $(\mu, \omega L/U)$ planes for the unforced problem with (———) and without (— — —) flag tension. The shaded zone in (a) marks the domain of stability. The cross and triangles correspond respectively to parameter combinations considered later in figures 3–5 and 6.

4.2. *Forced motion*

To demonstrate the relevance of the forced motion to the onset of motion, consider a flag of length $L = 1$ m and typical material properties as given after (3.2). In this case $\mu \approx 0.3$ and $\alpha \approx 40U$. According to figure 2(a), the critical value of α for the onset of motion in the absence of the pole wake is $\alpha_c \approx 14.8$ and the associated critical wind speed is $U_c \approx 0.4\,\mathrm{m\,s^{-1}}$. For a pole of diameter $D = 0.05$ m the resulting Reynolds number is $Re_D = UD/\nu \approx 1.3 \times 10^3$, considerably above the threshold value for vortex shedding from the pole, $Re_{D_{cr}} \sim 100$. This threshold value can be used to obtain the following condition for the onset of forced motion,

$$\alpha \geqslant \frac{L}{D}\sqrt{\frac{\rho_s \nu^2}{EI}}\, Re_{D_{cr}}. \tag{4.1}$$

Substituting $Re_{D_{cr}} = 100$, $D/L = 0.05$ and the above-mentioned values for a thin polyester flag ($\lambda = 10^{-4}$ m, $\rho_s \approx 0.4$ kg m^{-2}, $E = 3$ GPa), we find that the condition for onset of forced motion in this case is $\alpha \gtrsim 1.2$, valid for all $\mu(\approx 0.3/L)$. This value is significantly lower than the critical values calculated from homogeneous flag theory (figure 2a). Vortex shedding from the flag pole can therefore induce flapping even when the 'homogeneous' flag is nominally stable. This will be illustrated in the following where we focus on the forced motion at subcritical conditions of figure 2.

For a pole of diameter D at $Re_D \gg 1$ the vortices convect along $y = \pm h \approx \pm 0.45D$ (Griffin & Ramberg 1975; Blevins 1990).Using the estimates $\Gamma \approx 2.5UD$, $f_0 \approx 0.2U/D$,

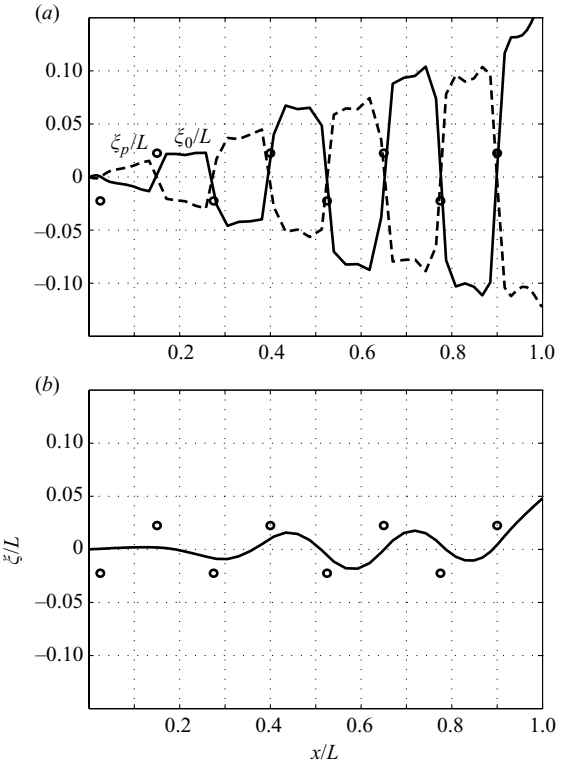

FIGURE 3. The profile of the flag at $Ut/L = 0.15$ for $D/L = 0.05$, $\mu = 0.3$ and $\alpha = 5$. (*a*) The 'vortex-induced' (ξ_p/L, – – –) and 'self' (ξ_o/L, ———) deflections; (*b*) the total deflection $\xi/L = \xi_p/L + \xi_o/L$. The circles denote the instantaneous location of vortices. The parameter combination considered is denoted by the cross in figure 2(*a*).

the non-dimensional representations of $\bar{\xi}_o$ and $\bar{\xi}_p$ in (3.16)–(3.17) become

$$\bar{\xi}_o(\bar{x}, \bar{t} - \bar{x}) \approx \frac{5D}{L} \sum_{n=0}^{\infty} (\mathrm{Re}\{\bar{\zeta}(\bar{x}, \bar{\omega}_n)\} \sin[\bar{\omega}_n(\bar{t} - \bar{x})] + \mathrm{Im}\{\bar{\zeta}(\bar{x}, \bar{\omega}_n)\} \cos[\bar{\omega}_n(\bar{t} - \bar{x})]) \exp\left[-\frac{9\bar{\omega}_n D}{20L}\right], \quad (4.2)$$

and

$$\bar{\xi}_p(\bar{x}, \bar{t} - \bar{x}) \approx \frac{5D\bar{x}}{L} \sum_{n=0}^{\infty} \sin[\bar{\omega}_n(\bar{t} - \bar{x})] \exp\left[-\frac{9\bar{\omega}_n D}{20L}\right], \quad (4.3)$$

where $\bar{\omega}_n = (2n + 1)2\pi L/5D$. Typically, $D/L \lesssim 0.1$ and the forced motion is characterized by flag oscillations of frequency $O(U/D)$. The magnitude of the high-frequency terms in the expansions ($n \gg 1$) decreases exponentially fast, and only a small number of terms ($n \lesssim 10$) is required for effective convergence for all parameter combinations studied here. With increasing D/L (corresponding to either a larger pole or a shorter flag), the vortex strength ($\approx 2.5UD$) increases and flag deflection is expected to increase. The dependence of the forced motion on the non-dimensional flag mass μ and the normalized wind speed α is contained in the component $\bar{\zeta}(\bar{x}, \bar{\omega})$ of the solution (4.2).

Figure 3 presents the flag profile obtained at time $\bar{t} = Ut/L = 0.15$ for $D/L = 0.05$ when $\mu = 0.3$ and $\alpha = 5$ (corresponding to the cross in figure 2*a*). Figure 3(*a*) shows

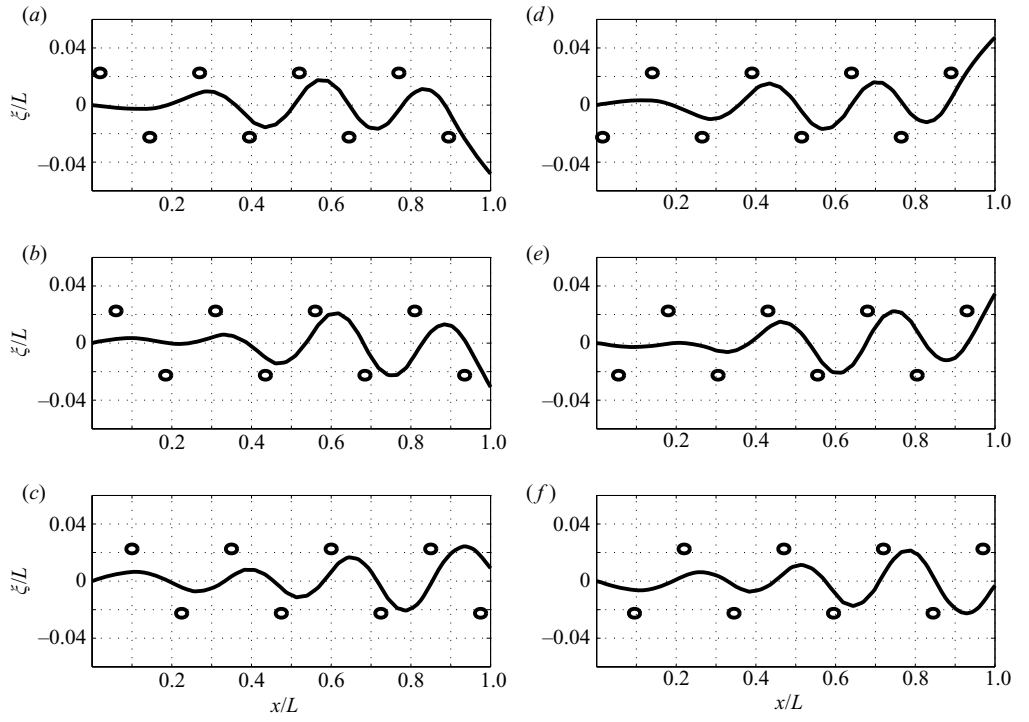

FIGURE 4. Time 'snapshots' of the flag profile ξ/L for $D/L=0.05$, $\mu=0.3$ and $\alpha=5$ over a single period ($0 \leqslant Ut_0/L < 0.25$) at $Ut/L=$ (*a*) 0.02, (*b*) 0.06, (*c*) 0.1, (*d*) 0.14, (*e*) 0.18 and (*f*) 0.22. The circles denote the instantaneous location of vortices. The parameter combination considered is denoted by the cross in figure 2(*a*).

the 'vortex-induced' $\bar{\xi}_p$ (dashed line) and the corresponding flag 'reaction' $\bar{\xi}_o$ (solid curve) and figure 3(*b*) shows the total deflection $\bar{\xi}=\bar{\xi}_o+\bar{\xi}_p$. The circles depict the instantaneous location of vortices released on opposite sides of the flag at non-dimensional intervals of time $Ut_0/2L=5D/2L=0.125$. When a vortex convects along the top or bottom sides of the flag, it produces rotational velocity that displaces the fluid around it. In particular, at the undisturbed flag plane $y=0$, each vortex 'pulls' the fluid behind it and 'pushes' the fluid in front of it, in accordance with the direction of the vortices indicated in figure 1. This local behaviour is visible in the 'vortex-induced' deflection (dashed line) in figure 3(*a*). The 'self' deflection (solid line) acts, as a 'reaction', in the opposite direction. The total local deflection induced by each vortex is clearly observed in figure 3(*b*) for the total deflection which increases in magnitude with increasing distance from the flag pole. The resulting motion, which can be roughly described as a superposition of such convecting 'ripples', is also illustrated in figure 4, where six consecutive time 'snapshots' of the flag profile $\bar{\xi}$ are plotted over a single period ($0 \leqslant Ut/L < 0.25$).

To study the time variation of the forced motion, the following discussion is framed in terms of the motion of the free end $x/L=1$, whose deflection is typically the largest along the flag. Figure 5 complements figures 3 and 4 by showing the free-end motion for the same parameters $D/L=0.05$, $\mu=0.3$ and $\alpha=5$. The time interval $0 \leqslant Ut/L \leqslant 1$ corresponds to two periods of the motion ($2t_0$) and a vortex passes the free end every $Ut_0/2L=0.125$. This is reflected by the symmetry properties of the 'vortex-induced' motion $\bar{\xi}_p$ (dashed line) and the corresponding flag 'reaction' $\bar{\xi}_o$

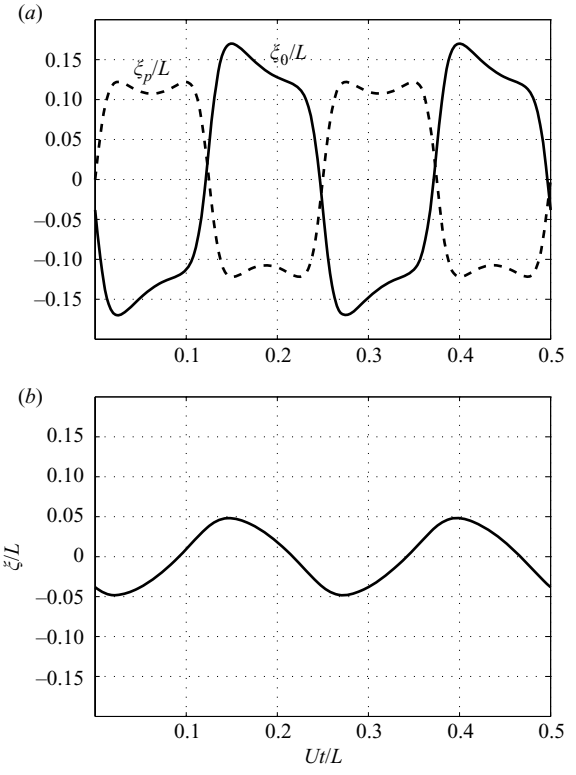

FIGURE 5. The forced motion of the free end ($x/L=1$) for $D/L=0.05$, $\mu=0.3$ and $\alpha=5$. (a) The 'vortex-induced' (ξ_p/L, – – –) and 'self' (ξ_o/L, ———) motions; (b) the total deflection $\xi/L=\xi_p/L+\xi_o/L$. The parameter combination considered is denoted by the cross in figure 2(a).

(solid curve) shown in figure 5(a). Their superposition $\bar{\xi}_o$ takes the simple wave-like pattern shown in figure 5(b).

It is expected that reduced wind speed and/or increased flag mass will result in motions of decreased amplitude, in accordance with our conclusion after (3.14): for either small α ('weak' wind) or large μ ('heavy' flag) the ratio of magnitudes $O(\alpha^2/\mu)$ between the fluid loading and bending stiffness terms in the equation of motion is small (see (3.1)). The motion is therefore dominated by flag inertia and by bending stiffness, causing the 'self' reaction $\bar{\xi}_o$ to cancel the 'vortex-induced' motion $\bar{\xi}_p$ so that the total deflection $\bar{\xi}\approx 0$. Yet, at every finite combination of α and μ there is a non-zero forced deflection, regardless of the stability properties of the flag discussed in § 4.1.

A comparison between the forced motion of relatively 'rigid' ($\alpha=1$) and 'flexible' ($\alpha=8$) flags for $\mu=0.3$ and $D/L=0.05$ is depicted in figure 6 (the respective (μ,α) combinations are marked by the triangles in figure 2a). In the 'rigid' ($\alpha=1$) case (figures 6a,b), $\bar{\xi}_o$ is almost equal and opposite to $\bar{\xi}_p$ (the latter being independent of μ and α and determined only by the ratio D/L; see (4.3)). The amplitude of the resulting free-end deflection $\bar{\xi}$ is therefore small. In the opposite case of a 'flexible' ($\alpha=8$) flag (figures 6c,d), large differences between $\bar{\xi}_p$ and $\bar{\xi}_o$ are followed by considerably larger amplitudes for $\bar{\xi}$. Similar results are obtained when comparing the forced motion of 'heavy' and 'light' flags.

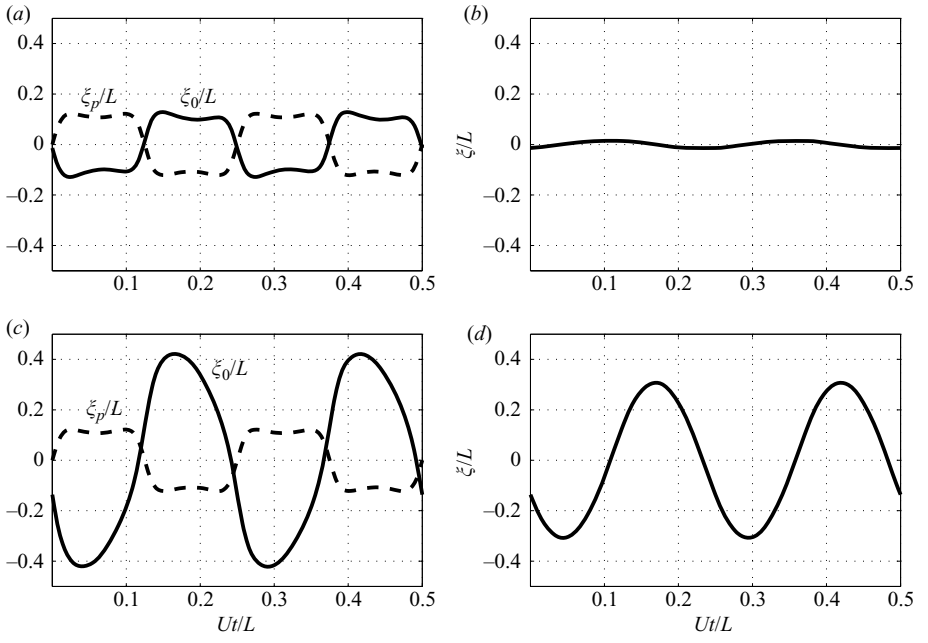

FIGURE 6. The effect of normalized wind speed (a, b) $\alpha = 1$ and (c, d) $\alpha = 8$ on the free-end ($x/L = 1$) deflection for $D/L = 0.05$ and $\mu = 0.3$. (a, c) The 'vortex-induced' (ξ_p/L, – – –) and 'self' (ξ_o/L, ———) motions; (b, d) the total deflection $\xi/L = \xi_p/L + \xi_o/L$. The parameter combinations considered correspond to the triangles in figure 2(a).

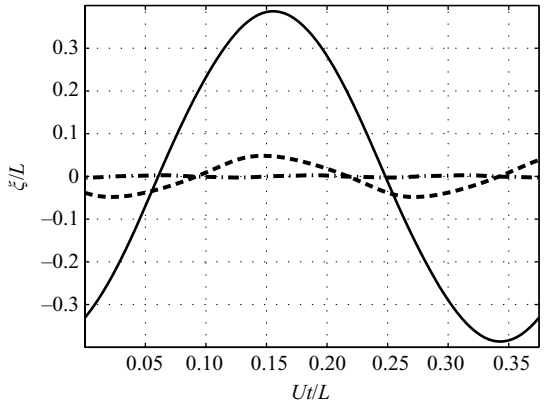

FIGURE 7. The effect of $D/L = 0.075$ (———), 0.05 (– – –) and 0.025 (– · – · –·) on the free-end ($x/L = 1$) deflection for $\mu = 0.3$ and $\alpha = 5$.

To illustrate the influence of the ratio D/L of pole diameter to flag length on the forced motion, we present in figure 7 the total deflection $\bar{\xi}$ of the free end for $D/L = 0.075$ (solid), 0.05 (dashed) and 0.025 (dash-dotted) when $\mu = 0.3$ and $\alpha = 5$. The value of D/L affects $\bar{\xi}_p$ both through its amplitude (because of the non-dimensional strength of the vortices $\approx 2.5D/L$) and frequency $\bar{\omega}_n \propto L/D$ (see (4.3)). Similarly, the 'self' deflection $\bar{\xi}_o$ is affected explicitly through its amplitude and frequency and implicitly owing to the $\bar{\omega}_n$-dependence of $\bar{\zeta}$ (see (4.2)). The results confirm that larger forced deflections occur when D/L is larger and that the frequency of flapping decreases with increasing D/L.

5. Conclusion

A real flag attached to a cylindrical pole of finite diameter and subject to a real wind will inevitably be driven by vortex shedding from the flag pole. Analyses of such problems based on ideal, homogeneous flag theory are therefore of little practical significance. For experimental studies, however, the importance of homogeneous flag theory is perhaps less certain. For a flag in air (or water) we can imagine a regime where the speed of a carefully controlled, effectively turbulence free, mean stream is gradually increased and where a flag is carefully pre-positioned parallel to the stream so that it is initially at rest. If the flag is pinned at a suitably 'streamlined' support exciting no vortex shedding, then the initial motions of the flag could well be in accord with the linear homogeneous theory. When the flag is pinned to a pole, on the other hand, vortex shedding will typically occur from the pole at mean flow speeds that are substantially subcritical, i.e. at which the homogeneous theory would predict a stable behaviour. The subsequent motion of the flag would then be described by the present theory of 'forced' excitation. At higher mean flow speeds the motion must become more complex and account must be taken of both forcing by the vortex wake of the flag pole and of possible contributions from the unstable motion of the flag. At this stage, nonlinear effects, which have been neglected in this work (justified by the small amplitudes of motion obtained in figures 3–7), should be considered.

Our theory has made several approximations, including the use of the Argentina-Mahadevan model (Argentina & Mahadevan 2005) to describe fluid loading and a simplified representation of vortex shedding that neglects, in particular, the back-reaction of the flag on the motion of the vortices. Essentially, these are details that can be amended by more careful and numerically more involved treatments that are not, however, expected to change the qualitative conclusions of this paper. In any event, when analysing the stability of a real flag it is evidently not acceptable to neglect the influence of the flag pole on the motion.

Appendix A. The problem for $\bar{\zeta}(\bar{x}, \bar{\omega})$

Substitute (3.11)–(3.13) into (3.6) together with (3.7) yields the equation

$$\begin{aligned}
&-\bar{\omega}^2\bar{\zeta} + \frac{1}{\alpha^2}[\bar{\zeta}'''' + 4\mathrm{i}\bar{\omega}\bar{\zeta}''' - 6\bar{\omega}^2\bar{\zeta}'' - 4\mathrm{i}\bar{\omega}^3\bar{\zeta}' + \bar{\omega}^4\bar{\zeta}] \\
&\quad -\frac{c_*}{\mu}[-\bar{\zeta}' - \mathrm{i}\bar{\omega}\bar{\zeta} + (1-\bar{x})(\bar{\zeta}'' + 2\mathrm{i}\bar{\omega}\bar{\zeta}' - \bar{\omega}^2\bar{\zeta})] - \frac{1}{\mu}\Delta\bar{\Pi} \\
&= \bar{\omega}^2\bar{x} - \frac{1}{\alpha^2}[-4\mathrm{i}\bar{\omega}^3 + \bar{\omega}^4\bar{x}] + \frac{c_*}{\mu}[-1 - \mathrm{i}\bar{\omega}\bar{x} + (1-\bar{x})(2\mathrm{i}\bar{\omega} - \bar{\omega}^2\bar{x})],
\end{aligned} \tag{A 1}$$

where

$$\Delta\bar{\Pi}(\bar{x}, \bar{\omega}) = -2C(\bar{\omega})\sqrt{\frac{1-\bar{x}}{\bar{x}}}\bar{\zeta}' + 2\bar{\omega}^2\sqrt{\bar{x}(1-\bar{x})}\bar{\zeta}. \tag{A 2}$$

Substitute (3.12)–(3.13) into (3.14) to obtain the end conditions

$$\begin{aligned}
&\bar{\zeta}(0) = 0, \\
&\bar{\zeta}''(0) + 2\mathrm{i}\bar{\omega}\bar{\zeta}'(0) = -2\mathrm{i}\bar{\omega}, \\
&\bar{\zeta}''(1) + 2\mathrm{i}\bar{\omega}\bar{\zeta}'(1) - \bar{\omega}^2\bar{\zeta}(1) = -2\mathrm{i}\bar{\omega} + \bar{\omega}^2, \\
&\bar{\zeta}'''(1) + 3\mathrm{i}\bar{\omega}\bar{\zeta}''(1) - 3\bar{\omega}^2\bar{\zeta}'(1) - \mathrm{i}\bar{\omega}^3\bar{\zeta}(1) = 3\bar{\omega}^2 + \mathrm{i}\bar{\omega}^3.
\end{aligned} \tag{A 3}$$

REFERENCES

Alben, S. & Shelley, M. J. 2008 Flapping states of a flag in an inviscid fluid: bistability and the transition to chaos. *Phys. Rev. Lett.* **101**, 119902.

Allen, J. J. & Smits, A. J. 2001 Energy harvesting eel. *J. Fluids Struct.* **15**, 629–640.

Argentina, M. & Mahadevan, L. 2005 Fluid-flow-induced flutter of a flag. *Proc. Natl Acad. Sci.* **102**, 1829–1834.

Beal, D. N., Hover, F. S., Triantafyllou, M. S., Liao, J. C. & Lauder, G. V. 2006 Passive propulsion in vortex wakes. *J. Fluid Mech.* **549**, 385–402.

Bisplinghoff, R. L., Ashley, H. & Halfman, R. L. 1955 *Aeroelasticity*. Addison-Wesley.

Blevins, R. D. 1990 *Flow-Induced Vibration*. Van Nostrand Reinhold.

Connell, B. H. & Yue, D. K. P. 2007 Flapping dynamics of a flag in a uniform stream. *J. Fluid Mech.* **581**, 33–67.

Eldredge, J. D. & Pisani, D. 2008 Passive locomotion of a simple articulated fish-like system in the wake of an obstacle. *J. Fluid Mech.* **607**, 279–288.

Eloy, C., Lagrange, R., Souilliez, C. & Schouveiler, L. 2008 Aeroelastic instability of cantilevered flexible plates in uniform flow *J. Fluid Mech.* **611**, 97–106.

Fitt, A. D. & Pope, M. P. 2001 The unsteady motion of two-dimensional flags with bending stiffness. *J. Engng Math.* **40**, 227–248.

Griffin, O. M. & Ramberg, S. E. 1975 On vortex strength and drag in bluff-body wakes. *J. Fluid Mech.* **69**, 721–728.

Hinze, J. O. 1975 *Turbulence*. McGraw-Hill.

Huang, L. 1995 Flutter of cantilevered plates in axial flow. *J. Fluids Struct.* **9**, 127–147.

Liao, J. C., Beal, D. N., Lauder, G. V. & Triantafyllou, M. S. 2003 Fish exploiting vortices decrease muscle activity. *Science* **302**, 1566–1569.

Lighthill, M. J. 1958 *An Introduction to Fourier Analysis and Generalized Functions*. Cambridge University Press.

Manela, A. & Howe, M. S. 2009 On the stability and sound of an unforced flag. *J. Sound Vib.* **321**, 994–1006.

Milne-Thomson, L. M. 1968 *Theoretical Hydrodynamics*. Macmillan.

Païdoussis, M. P. 1998 *Fluid-Structure Interaction: Slender and Axial Flow*. Academic.

Peyret, R. 2002 *Spetral Methods for Incompressible Viscous Flow*. Springer.

Rayleigh, J. W. S. 1945 *The Theory of Sound*. Dover.

Shelley, M., Vandenberghe, N. & Zhang, J. 2005 Heavy flags undergo spontaneous oscillations in in flowing water. *Phys. Rev. Lett.* **94**, 094302.

Shen, L., Zhang, X., Yue, D. K. P. & Triantafyllou, M. S. 2003 Turbulent flow over a flexible wall undergoing a streamwise travelling wave motion. *J. Fluid Mech.* **484**, 197–221.

Taneda, S. 1968 Waving motions of flags. *J. Phys. Soc. Japan* **24**, 392-401.

Tang, L. & Païdoussis, M. P. 2007 On the instability and the post-critical behaviour of two-dimensional cantilevered flexible plates. *J. Sound Vib.* **305**, 97–115.

Taylor, G. W., Burns, J. R., Kammann, S. M., Powers, W. B. & Welsh T. R. 2001 The energy harvesting eel: a small subsurface ocean/river power generator. *IEEE J. Ocean. Engng* **26**, 539–547.

Theodorsen, T. 1935 General theory of aerodynamic instability and the mechanism of flutter. *Tech. Rep.* No. 496, NACA.

Watanabe, Y., Isogai, K., Suzuki, S. & Sugihara, M. 2002*a* A theoretical study of paper flutter. *J. Fluids Struct.* **16**, 543–560.

Watanabe, Y., Suzuki, S., Sugihara, M. & Sueoka, Y. 2002*b* An experimental study of paper flutter. *J. Fluids Struct.* **16**, 529–542.

Zhang, J., Childress, S., Libchaber A. & Shelley, M. 2000 Flexible filaments in a flowing soap film as a model for one-dimensional flags in a two-dimensional wind. *Nature* **408**, 835–839.

Zhu, L. & Peskin, C. S. 2002 Simulation of a flapping Flexible filament in a flowing soap film by the immersed boundary method. *J. Comput. Phys.* **179**, 452–468.